Enhanced iterative egg-shape fitting to discretized object boundaries

Jiří Hladůvka[1,2*] and Walter G. Kropatsch[1]

[1*] Institute of Visual Computing and Human-Centered Technology, TU Wien, Favoritenstrasse 9–11, Vienna, A-1040, Austria.
[2*] Department of Applied Informatics, Comenius University, Mlynská dolina, Bratislava, 84248, Slovakia.

*Corresponding author(s). E-mail(s): jiri@prip.tuwien.ac.at;

Abstract

This paper presents an iterative method for fitting egg-shapes to discrete boundaries of objects. Egg-shapes extend ellipses by assigning a weight to one of the two focal points, resulting in a more pointed side. Fitting egg-shapes involves optimizing six parameters, but our approach simplifies this process to a one-dimensional parameter space.
First, we fit an ellipse and identify which principal semi-axis aligns with the more pointed side of the object. While the ellipse shares approximate position, size, and orientation with the desired egg-shape, fine-tuning the fit requires more than just adjusting the focal weight. We establish a relationship between the ellipse's eccentricity and the two parameters that define the closest egg-shapes. By leveraging this relationship, we iterate over a one-dimensional space of egg-shape candidates to assess their fit to the boundary, avoiding exhaustive methods.
Our results highlight the advantages of using egg-shapes over ellipses for representing a variety of real-world objects.

Keywords: egg-shape; fitting; discrete shape; eccentricity; ellipse; generalized conics.

1 Introduction

The core task in any computer vision problem is to define and efficiently express the essential object characteristics [14]. In order to represent a shape, one strategy is to approximate it by fitting a geometric primitive to the set of its boundary points. For example, an ellipse enables describing the 2D shape by elongation and orientation and requires 5 parameters. This significantly simplifies the processing and memory costs compared to the entire collection of pixels [2]. As a result, ellipse fitting is an area of extensive research [3, 7, 15, 20] and finds its use in a multitude of applications [10, 12, 13, 17].

This paper presents an advancement in the field of shape representation by exploring the potential of an *egg-shape* [5], i.e., a generalization of the ellipse with a weighted focal point. Despite the broadened scope of objects that might be described by egg-shapes, there are two key areas that have not been addressed to the best of our knowledge. Firstly, there is a lack of real-world examples demonstrating the benefits of egg-shapes. Secondly, it is the absence of a method for fitting egg-shapes to object boundaries. To this end, existing literature provides fitting methods for a different generalization, i.e., the super-ellipse [21, 11], that yields shapes from four-armed stars with concave sides to rectangles thru an additional parameter.

Addressing these gaps, we have identified various classes of real-world objects, such as chicken eggs, avocados, leaves, spoons, and rackets, that demonstrably benefit from egg-shape representation. We have assembled a collection of 1337 such objects, complete with photographs and boundaries, and have made this collection publicly accessible [18] in conjunction with the publication of this paper. A selection of four boundaries from this collection is presented in the results section 6.

The fitting algorithm could draw inspiration from constrained optimization techniques, as proposed for ellipses [4, 3, 7]. However, this approach requires a deep understanding of the interplay between egg-shape parameters and careful design of appropriate constraints. Furthermore, it would likely result in a multi-dimensional optimization problem with non-linear inequalities, leading to potential computational complexity and numerical instability.

Instead, we previously proposed an algorithm [9] that iteratively adjusts the special-case egg-shape, specifically the object-fitting ellipse, while constraining its two shape-defining parameters. In this work, we extend the algorithm in two key ways. First, we develop a procedure to identify the pointed side of the object, which effectively halves the number of iterations. Second, we leverage insights into the behavior of the objective function to move away from an exhaustive search. The resulting algorithms are detailed in section 4, and the corresponding research code is made publicly available [8].

The primary contribution of our work, detailed in section 3, is the reduction of the search space from six parameters to a single one. This was enabled by our key discovery, i.e., the relationship between egg-shape parameters and the eccentricity of its best-fitting ellipse. This contribution was facilitated by addressing two crucial aspects of the egg-shape: its *explicit*, polar-form representation (sec. 2.1) and the derivation of its arc-length sampling (sec. 2.2).

2 Egg-shapes

Conics have been generalized by assigning real-valued weights w_i to multiple focal points F_i in higher-dimensional metric spaces [6]. These generalizations are elegantly encompassed by $\Sigma_i w_i \|P - F_i\| = c \in \mathbb{R}$, which implicitly defines the conic by its points P.

In this work, we focus on shapes in the Euclidean plane induced by two foci and two positive weights. After a weight normalization [5], we are left with a single weight μ from the unit interval.

Definition 1 (Egg-shape) *Given two distinct foci $F_0 \neq F_1$ in the Euclidean plane, weight $0 \leq \mu \leq 1$, and scaling factor $c \geq 1$.* Egg-shape *is a set of points P in the Euclidean plane fulfilling*

$$d_0 + \mu d_1 = c \cdot f \tag{1}$$

where $d_i = \|P - F_i\|$ are the distances of P from foci F_i and $f = \|F_1 - F_0\|$ is the focal distance.

Wherever context permits, we may use the term *egg* as a shorthand for egg-shape. Definition 1 encompasses circles ($\mu = 0$), ellipses ($\mu = 1$), as well as a spectrum of egg-like shapes with various sharpness (Figure 8), including those with sharp corner [5] at $c = 1$ (Figure 4).

2.1 Polar coordinates

To explicitly express the egg in polar coordinates, we consider the two foci at the origin $F_0 = [0, 0]^\top$ and on the positive horizontal axis, $F_1 = [f, 0]^\top$. Setting the focal distance $f = 1$ yields what we refer to as the unit egg U_{01} (Figure 1).

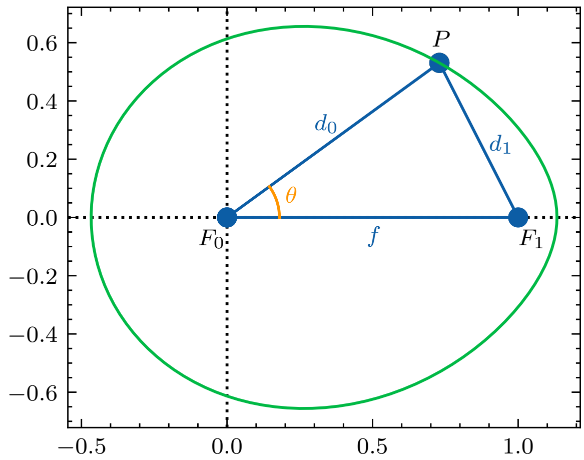

Fig. 1 Deriving polar coordinates. Unit egg U_{01} parametrized by $c = 1.2$, $\mu = 0.5$.

For any point P at angle θ on the egg (1) holds. Taking the square results in:

$$d_1^2 = \left(\frac{cf - d_0}{\mu}\right)^2 \tag{2}$$

Furthermore, the law of cosines yields:

$$d_1^2 = d_0^2 + f^2 - 2d_0 f \cos(\theta) \tag{3}$$

Subtracting (3) from (2) results in quadratic equation in d_0:

$$d_0^2\left(\mu^2 - 1\right) + d_0\left(2f(c - \mu^2\cos(\theta))\right) + f^2\left(\mu^2 - c^2\right) = 0. \tag{4}$$

For $\mu = 1$ the quadratic term vanishes yielding the polar equation of an ellipse. For $\mu = 0$, $d_0 = cf$ implicitly defines points P on a circle centered at F_0. For $0 < \mu < 1$ and fixed θ, the two solutions of (4), i.e.,

$$d_0^+, d_0^- = f \cdot \frac{\mu^2\cos(\theta) - c \pm \mu\sqrt{c^2 - 2c\cos(\theta) - \mu^2\sin^2(\theta) + 1}}{\mu^2 - 1} \tag{5}$$

correspond to distances (from F_0) of two points: P on the egg ($\mu > 0 \Rightarrow d_0^+$), and P^- on a generalized hyperbola ($\mu < 0 \Rightarrow d_0^-$) [5], which is further not discussed. Putting $r(\theta) = d_0^+$ yields the polar coordinates $(r(\theta), \theta)$ of the egg-shape.

2.2 Arc length

Similar to ellipses, uniform sampling of the polar angle θ will generally lead to uneven distribution of points on the boundary (Fig. 4, left). Such sampling would likely introduce bias when fitting to the discretized boundary of an object.

To address undersampled segments, we aim at the arc-length parameterization (Fig. 4, right). Computing the arc-length L between two angles $\theta_0 < \theta_1$ in the polar parametrization (r, θ) involves numerical integration of:

$$L(\theta_0, \theta_1) = \int_{\theta_0}^{\theta_1} \sqrt{r^2 + \left(\frac{dr}{d\theta}\right)^2}\, d\theta \tag{6}$$

Putting

$$R = R(\theta) = \sqrt{c^2 - 2c\cos(\theta) - \mu^2\sin^2(\theta) + 1} \tag{7}$$

$$M = M(\theta) = \mu^2\cos(\theta) - c \tag{8}$$

$$A = \mu^2 - 1 \tag{9}$$

simplifies the terms for r and its derivative w.r.t θ to:

$$r = f \cdot \frac{M + \mu R}{A} \tag{10}$$

$$\frac{dr}{d\theta} = -f \cdot \frac{M + \mu R}{A} \cdot \mu \cdot \frac{\sin(\theta)}{R} = -r \cdot \mu \cdot \frac{\sin(\theta)}{R} \tag{11}$$

Equation (11) confirms the discovery regarding the sharp corners [5] in eggs with $c = 1$ (Fig. 4). Specifically, when $c = 1$, $R(\theta)$ vanishes at $\theta = 2k\pi\ \forall k \in \mathbb{Z}$, which results in discontinuities in $dr/d\theta$ and leaves the derivatives undefined (Fig. 2). However, $dr/d\theta$ is an odd function with finite and opposing left/right limits in $2k\pi$:

$$\lim_{\substack{c=1 \\ \theta\to 2k\pi^-}} -r\mu\frac{\sin(\theta)}{R} = \frac{r\mu}{\sqrt{1-\mu^2}} = -\lim_{\substack{c=1 \\ \theta\to 2k\pi^+}} -r\mu\frac{\sin(\theta)}{R} \tag{12}$$

Therefore, the square $(dr/d\theta)^2$ in (6) exists in the limit (from either side):

$$\lim_{\substack{c=1 \\ \theta\to 2k\pi}} \left(\frac{dr}{d\theta}\right)^2 = \frac{r^2\mu^2}{1-\mu^2} \tag{13}$$

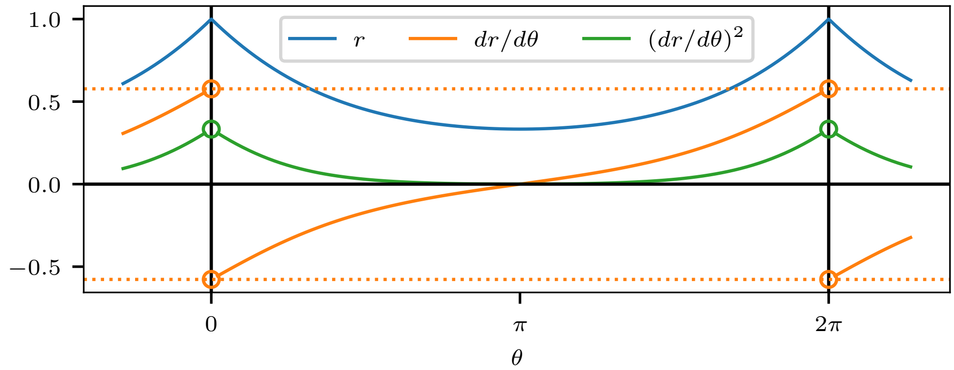

Fig. 2 While r is not differentiable w.r.t θ in the corner ($c = 1$, $\theta = 2k\pi$), its derivative $dr/d\theta$ has opposing left and right limits (12) displayed by hollow circles. The limit of the squared derivative therefore exists (13).

Equations (10)–(13) result, for given θ, in a recipe to reuse the radius r to compute the square of the derivative. Having the ingredients, both the arc-length $L(0, \theta)$ and its inverse can be numerically approximated (Fig. 3) and utilized to sample the egg points at regular distances (Fig. 4).

3 Egg-shapes and best-fitting ellipses

We aim to establish the correspondence between egg parameters and the eccentricity $\varepsilon = \varepsilon(c, \mu)$ of the best-fitting ellipse [7]. Two bounding cases are apparent from the equation for egg-shape (cf. Fig.5):

$\varepsilon(c, 0) = 0$: egg-shape, and thus also its best-fitting ellipse, is a circle implicitly given by $d_0 = cf$.

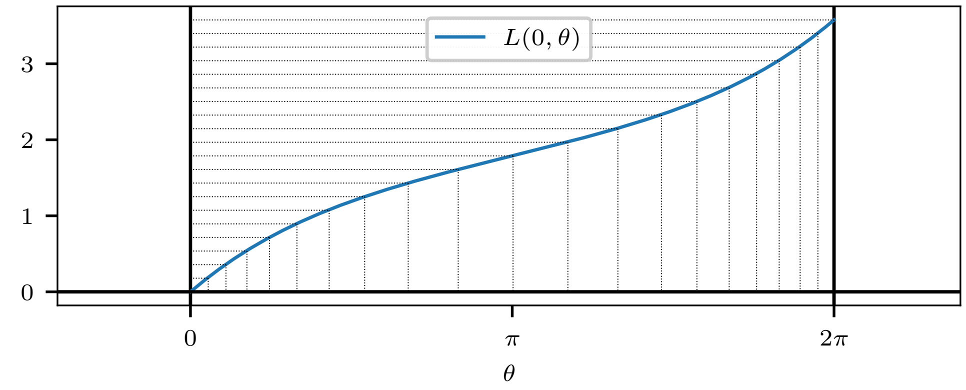

Fig. 3 Uniform sampling of the arc length $L(0, \theta)$ (horizontal lines) resulting in samples of the polar angle θ (vertical lines), which correspond to equidistant points on the egg-shape.

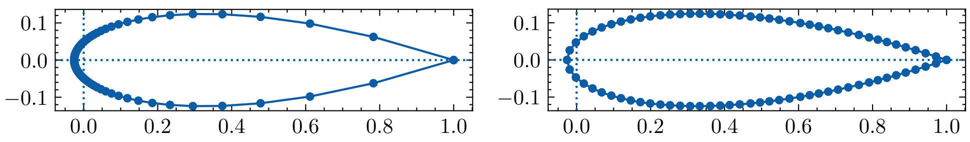

Fig. 4 A corner-egg ($c = 1$) with θ sampled linearly (left) and by arc length (right).

$\varepsilon(c, 1) = 1/c$: egg-shape, and thus also its best-fitting ellipse, is an ellipse implicitly given by $d_0 + d_1 = cf$, i.e., one with focal distance f, the length of its main axis cf, and eccentricity $\varepsilon = f/(cf) = 1/c$.

To model $\varepsilon(c, \mu)$ between we investigate the eccentricities of ellipses fitted to sampled unit egg boundaries, parametrized by c and μ. To explore the parameter space, we regularly sample $n_\mu = 49$ values for $\mu \in (0, 1)$ with step size of 0.02 and $n_c = 41$ values for $c \in \langle 1, 5 \rangle$ with step size of 0.1. Notably, the upper bound for c is determined by the expected lowest eccentricity of ellipses fitted to our modeled objects; specifically, $c_{\text{max}} = 1/\varepsilon_{\text{min}} \leq 5$. The robust ellipse-fitting algorithm [7] is employed for ellipse fitting.

Interestingly, this process reveals an increase of ε w.r.t. μ that follows a power law

$$\varepsilon \approx \frac{1}{c} \mu^{S_c} \tag{14}$$

for c-dependent exponents $S_c \in (0, 1)$. This can be seen in Fig. 5 by the two dotted curves at $c = 1$ and $c = 5$ as well as in Fig. 6 for 9 selected values of c.

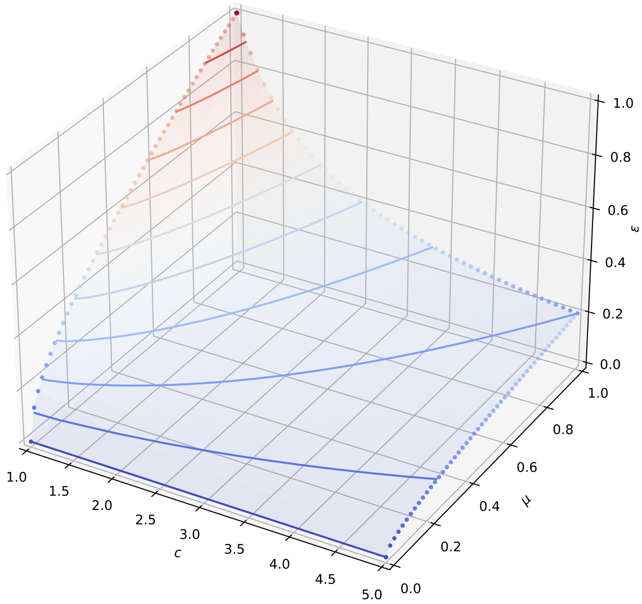

Fig. 5 Relationship between egg-shape parameters c,μ, and the eccentricity of the best-fitting ellipse. The ten solid curves correspond to iso-eccentricity lines (blue at 0, red at 0.9). The red dot at $(c,\mu) = (1,1)$ corresponds to the unit eccentricity of the degenerated case, i.e., the line connecting the two foci.

The power-like nature is better articulated in the log-log plot (Fig. 6, right) where the curves lend themselves to linear modeling:

$$\log \varepsilon \approx \log \left(\frac{1}{c} \mu^{S_c} \right) = S_c \log \mu - \log c \tag{15}$$

While these lines seem to be parallel, a closer inspection reveals their slopes S_c obtained as an average of the respective samples i:

$$S_c = \frac{1}{n_\mu} \sum_{i=1}^{n_\mu} \frac{\log \varepsilon_i + \log c}{\log \mu_i} = \frac{1}{n_\mu} \sum_{i=1}^{n_\mu} \frac{\log \varepsilon_i c}{\log \mu_i} \tag{16}$$

are inversely proportional to c (Fig. 7). This can be modeled by

$$S(c) \approx S(c; \alpha, \beta, \gamma) = \beta + \frac{\alpha}{c + \gamma}. \tag{17}$$

.

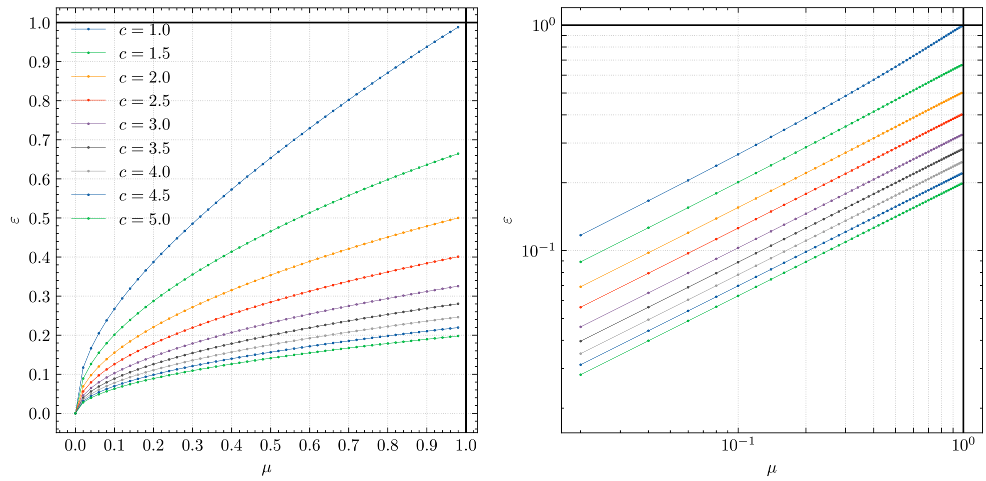

Fig. 6 Eccentricities ε of ellipses fitted to unit egg-shapes parametrized by (c, μ), for 9 selected values of $c \in \langle 1, 5 \rangle$ times 49 samples of $\mu \in (0, 1)$. The linear tendency of the samples in the log-log plot (right) informs a power-law modeling of the eccentricity curves w.r.t. μ.

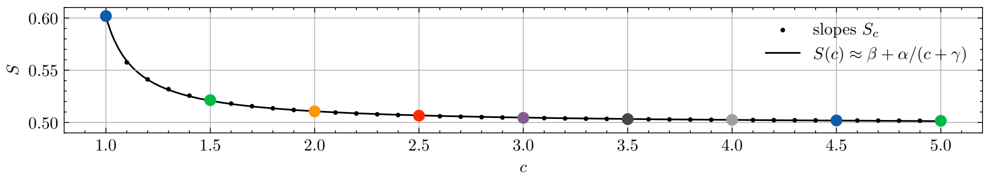

Fig. 7 Inversely proportional slopes S_c can be modeled by Eq. (17). The color dots correspond to the same values of c as shown in Fig. 6.

Putting the things together, we aim to model eccentricity

$$\varepsilon(c, \mu) \approx \frac{1}{c} \cdot \mu^{S(c)} \tag{18}$$

by fitting the three parameters parameters α, β, and γ to the eccentricities measured at the c, μ grid. The fitting results in $\alpha = 0.01994611$, $\beta = 0.49646579$, $\gamma = -0.7994735$ and yields an error in eccentricity of 0.0000 ± 0.0013.

It is worth mentioning that this modeling is performed only once, before fitting egg-shapes to object boundaries.

4 Fitting egg-shapes via an ellipse proxy

Equation (18) relates the eccentricity of best-fitting ellipse given egg-shape parameters. More importantly, we can constrain the inverse, egg-to-ellipse fitting problem to the iso-eccentricity curve in the (c, μ) space (Figure 8).

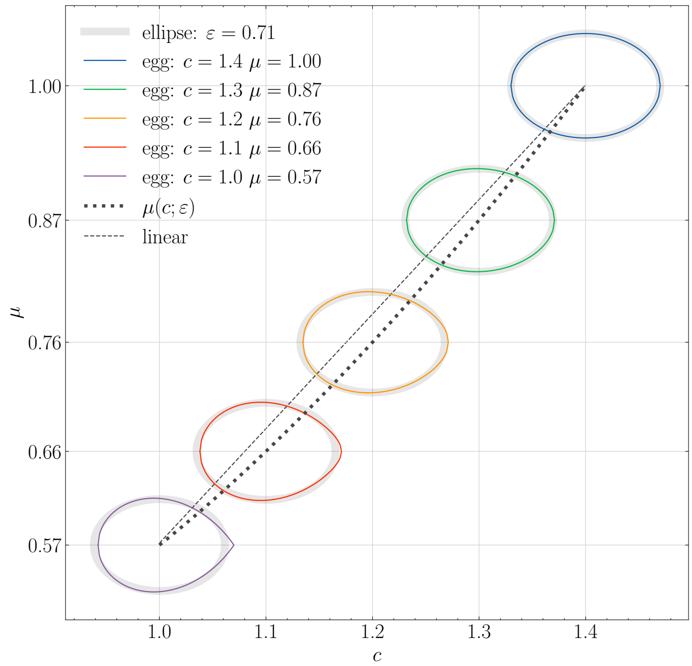

Fig. 8 Sampled best-fitting eggs to an ellipse of fixed eccentricity on the curve given by equation (19) in the (c, μ) parameter space. For clarity, the unit eggs are scaled down.

Given an ellipse of eccentricity ε, the parameter c is restricted to the interval $\langle 1, 1/\varepsilon)$. Rewriting (18) allows, for a fixed c, computation of the corresponding μ:

$$\mu = \mu(c;\varepsilon) = (c \cdot \varepsilon)^{1/S(c)} \approx (c \cdot \varepsilon)^{\frac{(c+\gamma)}{\beta(c+\gamma)+\alpha}} \tag{19}$$

Our objective is to fit an egg-shape to a segmented egg-like object represented by its boundary points B. It is important to note that, unlike the *unit* egg, the objects can be arbitrarily scaled, oriented, and placed within the Euclidean plane.

The steps of Algorithm 1 proceed as follows. We begin by fitting a *proxy* ellipse E_B to the boundary points B and recording its eccentricity ε_B. In addition to [9], FitEllipse also determines the orientation of its major semi-axis towards the more pointed end of B (see Appendix A for details). This adjustment simplifies and approximately halves the run-time of the previously published Algorithm 1 in [9] by eliminating its inner loop, which originally accounted for both semi-axis orientations.

Next, we conduct an iterative search along the iso-eccentricity curve. In each iteration, we fit an ellipse E_U to the arc-sampled unit egg U_{01}. Because both ellipses share the same eccentricity, they are similar. The corresponding similarity transform then aligns U_{01} with the boundary B (see Appendix A).

Finally, we assess this alignment by means of average Hausdorff distance, $\overline{HD}$, which is defined later in section 5.

Algorithm 1 Exhaustive egg fitting to boundary along 1D iso-eccentricity curve

Require: B ▷ boundary coordinates of egg-like object
1: $E_B \leftarrow$ FitEllipse (B) ▷ fit a proxy ellipse to the boundary
2: $\varepsilon_B \leftarrow$ eccentricity (E_B) ▷ eccentricity to restrict the search
3: $(\Delta^*, F_0^*, F_1^*, c^*, \mu^*) \leftarrow (\infty, [0,0]^\top, [1,0]^\top, 1, 0)$ ▷ loss, foci, and params to optimize
4: **for** $c \in \langle 1, 1/\varepsilon_B)$ **do** ▷ sample the iso-eccentricity curve
5: $\quad \mu \leftarrow \mu(c; \varepsilon_B)$ ▷ equation (19)
6: $\quad U_{01} \leftarrow$ unit_egg (c, μ) ▷ unit egg given by c, μ
7: $\quad E_U \leftarrow$ FitEllipse (U_{01}) ▷ ellipse fitting the unit egg ($\varepsilon_U \approxeq \varepsilon_B$)
8: $\quad T_{UB} \leftarrow \operatorname{argmin}_T |T(E_U), E_B|$ ▷ E_U to E_B alignment transform (25)
9: $\quad M \leftarrow T_{UB}(U_{01})$ ▷ transform the unit egg to the object boundary
10: $\quad \Delta \leftarrow \overline{HD}(M, B)$ ▷ distance of the transformed egg to the boundary
11: $\quad$ **if** $\Delta < \Delta^*$ **then** ▷ if loss decreased
12: $\quad\quad (\Delta^*, F_0^*, F_1^*, c^*, \mu^*) \leftarrow \big(\Delta,\ T_{UB}([0,0]^\top),\ T_{UB}([1,0]^\top),\ c, \mu\big)$ ▷ update
13: $\quad$ **end if**
14: **end for**
15: **return** $(F_0^*, F_1^*, c^*, \mu^*)$ ▷ foci and parameters of the best-fitting egg

The brute-force loop beginning on line 4 of Algorithm 1 requires discretizing the half-open interval $\langle 1, 1/\varepsilon_B)$, where in [9], we employed 50 equidistant samples to iterate over the parameter c.

To this end we propose another enhancement by analyzing the discrete error curves stemming from algorithm 1, specifically the Hausdorff distance as a function of $c \in \langle 1, 1/\varepsilon_B)$. This analysis was conducted on a test dataset [18] (further described in Section 5) and revealed that error curves exhibit a tendency toward either monotonic or convex behavior (Figure 9), occasionally perturbed by minor noise. Based on this observation, we reformulate the algorithm in a more modular fashion, enabling the substitution of the brute-force loop with a local optimization.

In algorithm 2, the two ellipses are described by 6-tuples $(x, y, a, b, \varepsilon, \phi)$ encoding center, lengths of main axes, eccentricity, and orientation. Constrained by the eccentricity ε_B of the object's proxy ellipse E_B, EggCandidate generates an egg shape at c, transformed to align with the object boundary B. Disregarding foci F_i and parameters c and μ of the egg shape, the Loss function evaluates the fitness of its boundary M against the object B.

Due to its discrete nature, computing or approximating the gradient of the compound loss on line 16 in FitEgg is challenging, if not impossible, necessitating the use of optimization algorithms that do not rely on gradient information. Knowing the nature of error curves and the bounds of c, we utilized the Brent's algorithm [1] to compute the argmin on line 16. As a result, we observed two notable improvements over equidistant sampling [9]: (1) the method identified more refined minima, and (2) it reduced the average number of EggCandidate calls to 23, leading to a 2.4-fold increase in computational efficiency (see also Figure 9).

Algorithm 2 Replacing exhaustive search

function EggCandidate(c, E_B)
    $\mu \leftarrow \mu(c, \varepsilon_B)$ ▷ $\varepsilon_B \in E_B$; equation (19)
    $U_{01} \leftarrow$ unit_egg (c, μ) ▷ unit egg given by c, μ
    $E_U = (x_U, 0, a_U, b_U, \varepsilon_U, 0) \leftarrow$ FitEllipse (U_{01}) ▷ ellipse fitting the unit egg
    $T_{UB} \leftarrow \text{argmin}_T |T(E_U), E_B|$ ▷ E_U to E_B ellipse alignment (25)
    $M \leftarrow T_{UB}(U_{01})$ ▷ transform unit egg boundary points
    $(F_0, F_1) \leftarrow \left(T_{UB}([0,0]^\top),\ T_{UB}([1,0]^\top)\right)$ ▷ transform the unit egg foci
    return $(F_0, F_1, c, \mu)\,, M$ ▷ model parameters and boundary points
end function

function Loss($(c, E_B), B$) ▷ measure model-to-object alignment
    $(F_0, F_1, c, \mu)\,, M \leftarrow$ EggCandidate(c, E_B)
    return $\overline{HD}(M, B)$ ▷ avgerage Hausdorff of boundaries (21)
end function

Require: B ▷ boundary coordinates of egg-like object
function FitEgg(B)
    $E_B = (x_B, y_B, a_B, b_B, \varepsilon_B, \phi_B) \leftarrow$ FitEllipse (B) ▷ proxy oriented at ϕ_B
    $c^* = \text{argmin}_{c \in \langle 1, 1/\varepsilon_B)}$Loss(EggCandidate($c, E_B$), B) ▷ find optimal c
    $(F_0^*, F_1^*, c^*, \mu^*)\,, M^* \leftarrow$ EggCandidate($c^*; E_B$) ▷ optimal egg-shape model
    return $(F_0^*, F_1^*, c^*, \mu^*)$ ▷ foci and parameters of the best-fitting egg
end function

5 Validation

Our methodology is verified using both overlap-centric and distance-centric metrics [19] on a purposely created collection of boundaries [18] segmented from images of both biological and common objects. These include both deformable and rigid items captured in arbitrary orientations and scales. Each segmentation is represented by a binary mask and its boundary thus as a set of integer coordinates.

5.1 Datasets

Whole eggs: Boundaries of 1,100 photographed eggs [16].
Boiled eggs: Images of longitudinally halved, hard-boiled eggs found on the internet were manually segmented, yielding 12 boundaries each for the egg whites and yolks.
Avocados: Images of longitudinally halved avocados were found on the internet. The shells of these avocados were manually segmented, resulting in 6 boundaries. Some of them are slightly deformed.
Leaves: Tree and plant leaves were deliberately selected and photographed in line with this study. The criteria included being longitudinally symmetrical, egg-shaped, elongated, and possibly pointed. Manual segmentation excluded the stems and produced 23 boundaries.
Cells: Palisade cells of Arabidopsis thaliana in a micro-CT cross-section slice were manually segmented, resulting in 159, mostly elliptic boundaries.

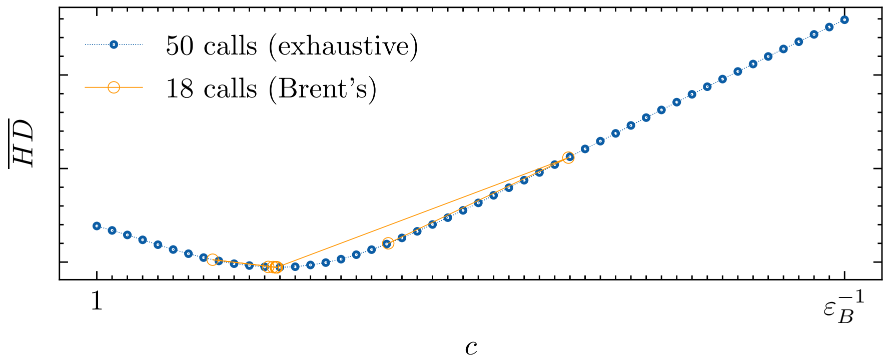

Fig. 9 An example of the iterative process for minimizing the Average Hausdorff Distance ($\overline{HD}$) with respect to the free egg-shape parameter $c \in \langle 1, 1/\varepsilon_B)$ by exhaustive search and Brent's algorithm. The two polylines represent the number and order of objective function calls.

Household items: 11 spoon heads and 2 toilet seats segmented from photos.
Rackets: Images of tennis, badminton, and squash racket heads sourced from the internet were segmented, resulting in 12 boundaries. The outer shell of the squash head is noted to be pointed. One of the tennis heads is elliptic.

5.2 Validation metrics

The geometric alignment of a model with the object boundary is evaluated using metrics that take into account either the boundary point sets M and B, or the corresponding polygons $\mathbf{M}$ and $\mathbf{B}$.

5.2.1 IoU

(also referred to as the Jaccard index) [19], defined as the area of the intersection divided by the area of the union of polygons $\mathbf{M}$ and $\mathbf{B}$:

$$IoU(M, B) = \frac{|\mathbf{M} \cap \mathbf{B}|}{|\mathbf{M} \cup \mathbf{B}|} \tag{20}$$

ranges from 0 to 1, with 1 indicating perfect alignment.

5.2.2 The Average Hausdorff Distance ($\overline{HD}$)

is used to assess the fitness for its decreased sensitivity to outliers [19] when compared to the usual Hausdorff distance. $\overline{HD}$ is defined by:

$$\overline{HD}(M, B) = \max\left(d(M, B), d(B, M)\right) \tag{21}$$

where d(X, Y) is the *directed* Average Hausdorff distance [19] given by:

$$d(X, Y) = \frac{1}{|X|} \sum_{x \in X} \min_{y \in Y} ||x - y||. \tag{22}$$

To assess improvements of egg models M_G over elliptic models E_L across contours of different lengths we further introduce the following normalization:

5.2.3 Normalized improvement (*NI*)

in average Hausdorff distance $\overline{HD}$ of egg model M_G over elliptical model M_L when fitted to boundary B. We define $NI = 0$ if models align. Otherwise:

$$NI(M_G, M_L|B) = \frac{\overline{HD}(M_L, B) - \overline{HD}(M_G, B)}{\max\left(\overline{HD}(M_L, B)\ ,\ \overline{HD}(M_G, B)\right)}. \tag{23}$$

Being already normalized, IoU is naturally suited to assess improvements by:

$$\Delta IoU(M_G, M_L|B) = IoU(M_G, B) - IoU(M_L, B). \tag{24}$$

Both improvement metrics fall in the closed interval $\langle -1, 1\rangle$. Positive values indicate an improvement due M_G, while negative values signify a decline.

6 Results

Figure 11 showcases a selection of top-improvement examples. To avoid clutter, Figure 10 summarizes both improvement metrics (23),(24) in two separate scatter plots. 94.68% of data points indicating improvements in both metrics are located in the 1^{st} quadrants. The ties in the 2^{nd} and 4^{th} quadrants correspond to cases improved in only one of the metrics. They account for $10 + 11$ out of 159 cells and $9 + 12$ out of 1100 whole eggs. Finally, the 3^{rd} quadrant shows minimal declines in both metrics: less than 4% of cells (6 out of 159) and less than 2% of whole eggs (20 out of 1100). The leftmost point of the upper part is the elliptic tennis racket that can not be improved by the egg-shape.

In the marginal-improvement rectangle $(0, 0.1) \times (0, 0.02)$ in the upper part, a cluster of 9 boiled-egg yolks can be found. They are almost elliptical making it difficult for the egg-shapes to improve them. This explains the almost identical IoU and only marginally improved NI values. The enclosed badminton racket already deviates from an ellipse and was slightly improved by an egg-shape.

Upon examining areas with higher improvements, it becomes apparent that the term *egg*-shapes may warrant reconsideration. In our selection, avocados outperformed eggs (both boiled and whole) in both metrics. This can be attributed to their more tapered shape, which is better modeled by egg-shapes.

A similar observation can be made about the top-scoring leaves (e.g., those with $\Delta IoU \gtrsim 0.06$) and spoons ($NI \gtrsim 0.6$), which are difficult to model using ellipses. However, egg-shapes have proven effective in modeling the spikes or even sharp corners by reducing c towards 1 (refer to Fig. 11).

In the bottom part of Fig. 10, most of the plant cells cluster in the marginal improvement rectangle. This is because most of the cells are elliptical or even circular in shape, and an ellipse already provides a good model. A strong correlation between the metrics is evident for both datasets. Unlike eggs, the cells have been

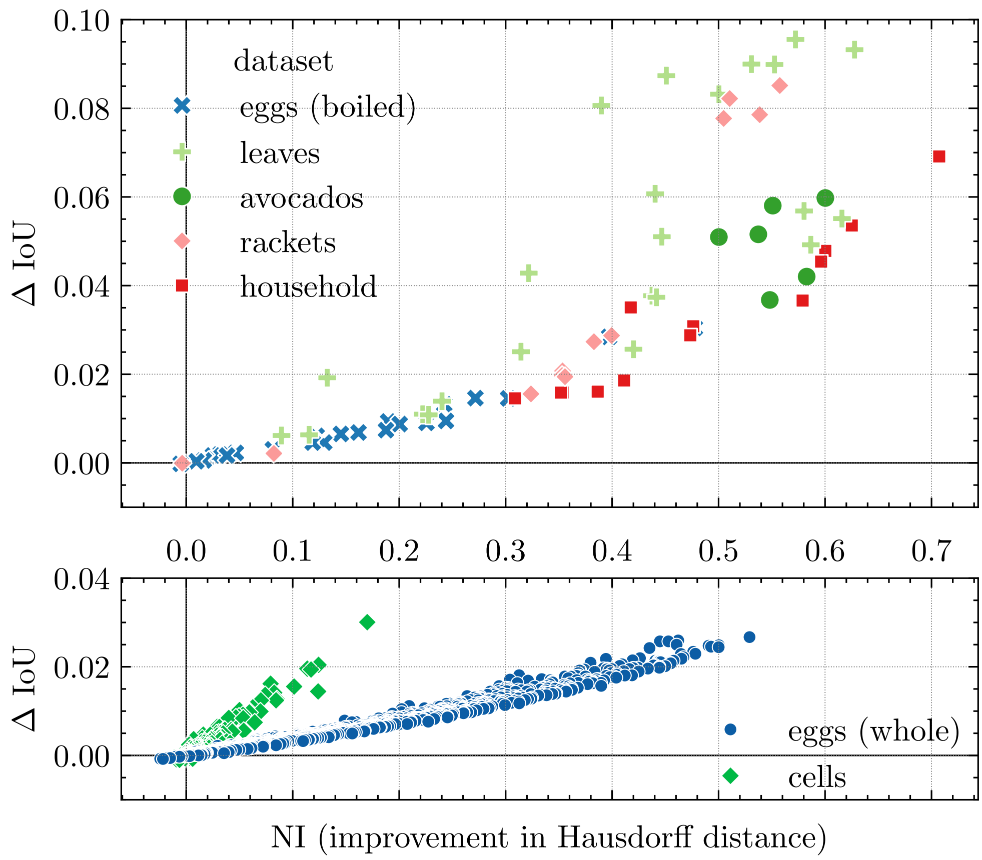

Fig. 10 Normalized improvements in average Hausdorff distance (NI) and in IoU.

segmented from a single image, which results in more jagged boundaries. For such boundaries, improvements in IoU could potentially be more pronounced than those in NI, explaining the steeper trend.

7 Conclusions and future work

In this paper, we introduced a novel method for fitting discrete boundaries using egg-shapes. We ventured beyond the confines of implicit equations and harnessed the power of explicit representation in conjunction with arc-length parametrization. This approach led to our key finding: a relationship between egg-shape parameters and the eccentricity of the best-fitting ellipse, which subsequently informed the design of our fitting algorithm.

Our algorithm was rigorously tested on over 1,000 boundaries. The results have demonstrated the potential of egg-shapes for representing real-world objects. Unexpectedly, we have discovered that there are objects other than *eggs*, which when fitted

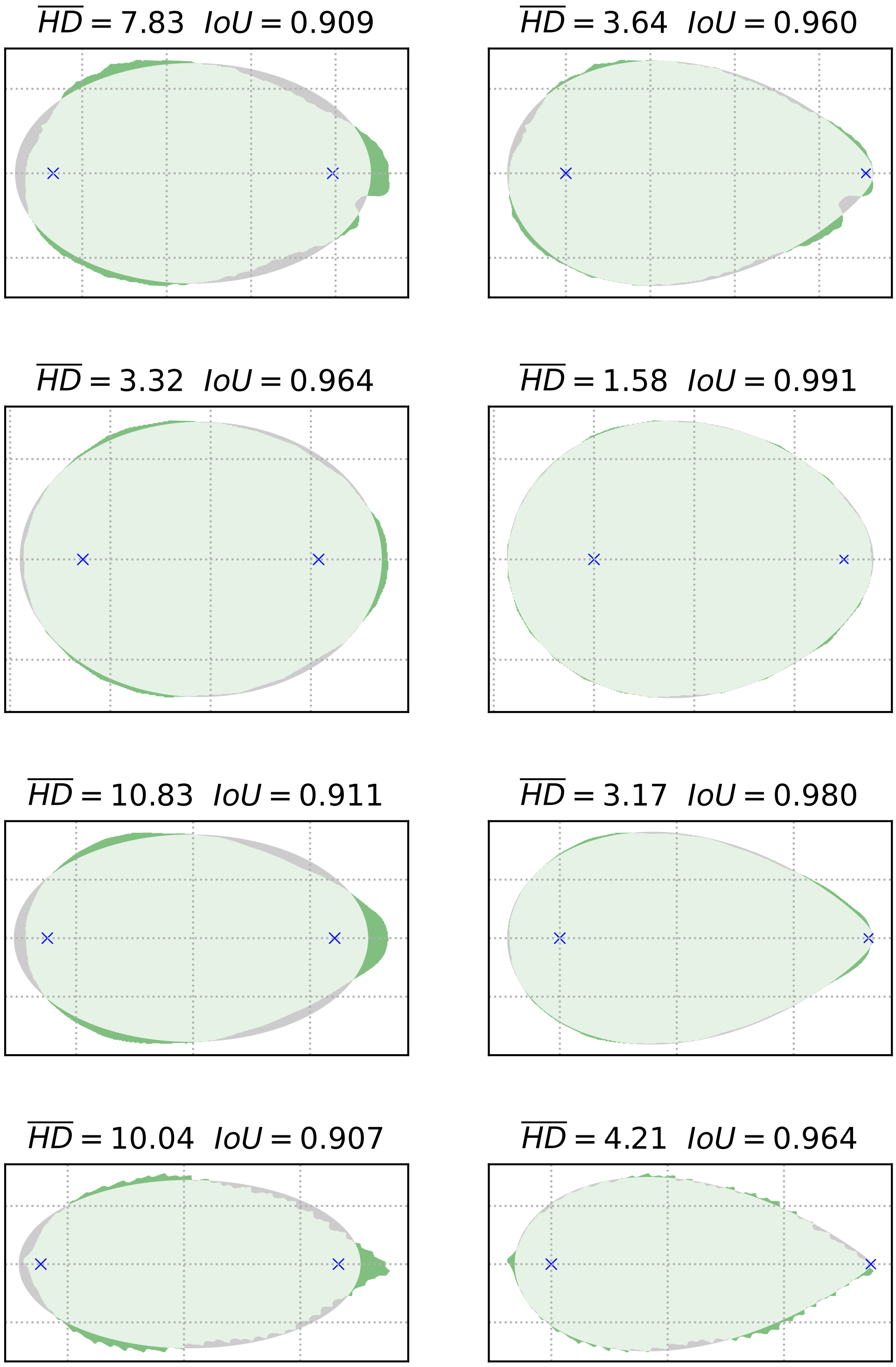

Fig. 11 Improvements by egg-shape fit (right column) over elliptic fit (left column) for selected contours. Top to bottom: avocado ($NI = 0.54$), whole egg ($NI = 0.52$), spoon head ($NI = 0.71$), and leaf ($NI = 0.58$). Gray and dark green areas are not explained well by the respective model. The blue crosses show the foci.

with an *egg*-shape, show even better improvements over elliptic fits. This intriguing finding expands the potential applications of egg-shape fitting beyond what was initially anticipated.

The results of our research pave the way for future development, which can be pursued along several avenues: 1. The choice of arc-length parametrization was largely based on intuition. A comparison with its linear counterpart is necessary to validate our approach. 2. Similar to egg-shape parameters, we observed a promising pattern between eccentricity and the offsets of the focal points. However, modeling this seems to be a more complex task. 3. We have yet to address the robustness of our method in dealing with noise, overlaps, or partial occlusions.

Acknowledgements

This work was supported by the Vienna Science and Technology Fund (WWTF) project LS19-013 and by the European Union's NextGenerationEU through the Recovery and Resilience Plan for Slovakia under the project 09I03-03-V04-00363. Computational resources were provided by the Vienna Scientific Cluster (VSC).

References

[1] Brent, R.P.: Chapter 5: An algorithm with guranteed convergence for finding a minimum of a function of one variable. In: Algorithms for Minimization Without Derivatives, pp. 61–80. Prentice-Hall (1973)

[2] Costa, L.d.F., Cesar Jr, R.M.: Shape analysis and classification: theory and practice. CRC Press (2000)

[3] Fitzgibbon, A., Pilu, M., Fisher, R.: Direct least square fitting of ellipses. IEEE Transactions on Pattern Analysis and Machine Intelligence **21**(5), 476–480 (1999)

[4] Fitzgibbon, A.W., Pilu, M., Fisher, R.B.: Direct least squares fitting of ellipses. In: Proceedings of 13th international conference on pattern recognition. vol. 1, pp. 253–257. IEEE (1996)

[5] Gabdulkhakova, A., Kropatsch, W.G.: Generalized conics with the sharp corners. In: Progress in Pattern Recognition, Image Analysis, Computer Vision, and Applications. pp. 419–429 (2021)

[6] Groß, C., Strempel, T.K.: On generalizations of conics and on a generalization of the Fermat–Torricelli problem. The American Mathematical Monthly **105**(8), 732–743 (1998)

[7] Halíř, R., Flusser, J.: Numerically stable direct least squares fitting of ellipses. In: 6th International Conference in Central Europe on Computer Graphics and Visualization (WSCG). pp. 125–132 (1998)

[8] Hladůvka, J.: Eggfit: An iterative algorithm to fit egg-shapes to object boundaries. Software stack, TU Wien (2024). https://doi.org/10.48436/2x212-zsv77

[9] Hladůvka, J., Kropatsch, W.G.: Fitting egg-shapes to discretized object boundaries. In: Brunetti, S., Frosini, A., Rinaldi, S. (eds.) Discrete Geometry and Mathematical Morphology. pp. 107–119. Springer Nature Switzerland, Cham (2024). https://doi.org/10.1007/978-3-031-57793-2_9

[10] Kanatani, K., Sugaya, Y., Kanazawa, Y.: Ellipse fitting for computer vision: Implementation and applications. Springer (2016)
[11] Köhntopp, D., Lehmann, B., Kraus, D., Birk, A.: Segmentation and classification using active contours based superellipse fitting on side scan sonar images for marine demining. In: IEEE International Conference on Robotics and Automation. pp. 3380–3387 (2015)
[12] Kothari, R.S., Chaudhary, A.K., Bailey, R.J., Pelz, J.B., Diaz, G.J.: Ellseg: An ellipse segmentation framework for robust gaze tracking. IEEE Transactions on Visualization and Computer Graphics **27**(5), 2757–2767 (2021)
[13] Liao, M., Zhao, Y.Q., Li, X.H., Dai, P.S., Xu, X.W., Zhang, J.K., Zou, B.J.: Automatic segmentation for cell images based on bottleneck detection and ellipse fitting. Neurocomputing **173**, 615–622 (2016)
[14] Loncaric, S.: A survey of shape analysis techniques. Pattern recognition **31**(8), 983–1001 (1998)
[15] Long, C., Hu, Q., Zhao, M., Li, D., Ouyang, Z., Yan, D.M.: A triple-stage robust ellipse fitting algorithm based on outlier removal. IEEE Transactions on Instrumentation and Measurement **72**, 1–14 (2023)
[16] Nho, T.: Egg-segmentation dataset. https://universe.roboflow.com/the-nho/egg-segmentation (mar 2023), visited on 2023-07-26
[17] Panagiotakis, C., Argyros, A.: Region-based fitting of overlapping ellipses and its application to cells segmentation. Image and Vision Computing **93**, 103810 (2020)
[18] Pelletier, V., Hladůvka, J.: Eggshapes: A collection of egg-shaped objects and their boundaries. Dataset, TU Wien (2023). https://doi.org/10.48436/de66n-2pj41
[19] Taha, A.A., Hanbury, A.: Metrics for evaluating 3D medical image segmentation: analysis, selection, and tool. BMC Medical Imaging **15**, 29 (2015)
[20] Wang, W., Wang, G., Hu, C., Ho, K.C.: Robust ellipse fitting based on maximum correntropy criterion with variable center. IEEE Transactions on Image Processing **32**, 2520–2535 (2023)
[21] Zhang, X., Rosin, P.L.: Superellipse fitting to partial data. Pattern Recognition **36**(3), 743–752 (2003)

A Unit-egg to boundary alignment

In each step of the iterative search, the unit egg candidate U_{01} is transformed by a similarity transformation to approximate the boundary B. This transformation is determined, up to orientation, by the two similar fitting ellipses E_U and E_B (Fig. 12).

To achieve consistency in orientations, we ensure that the major semi-axes of the ellipses point towards the more pointed part of the matched shapes. Following the definition of the unit egg we set its orientation to the positive x-axis. For the arbitrarily orientated egg-like shape B, we need a mechanism to determine which of the two semi-major axes heads towards its more pointed end.

Given the fitting ellipse E_B by its center $[x_B, y_B]^\top$, major-axis $\vec{a_B}$, and minor axis $\vec{b_B} \perp \vec{a_B}$ vectors, we split the boundary points B into two subsets B^+ and B^-, based on the half-planes defined by the center and the two opposing semi-axes orientations, i.e., $\vec{a_B}$ and $-\vec{a_B}$. We then project both subsets onto the minor axis $\vec{b_B}$ and compare their variances. The subset of the smaller variance indicates the semi-axis towards the more pointed tip of B. We denote its angle from the positive horizontal axis as ϕ.

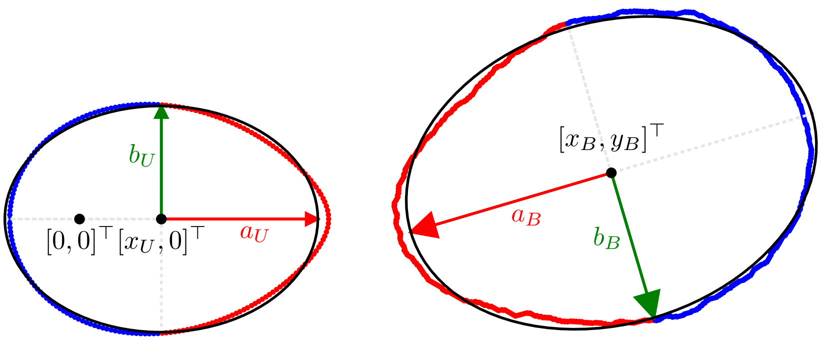

Fig. 12 Orientation of unit egg ellipse E_U (left) and boundary ellipse E_B (right). Projections of the red boundary part (B^+) onto minor axis b_B yield lower variance than projections of the blue counterpart (B^-).

The transformation of the axis-aligned ellipse E_U centered at $[x_U, 0]^\top$ to the similar ellipse E_B centered at $[x_B, y_B]^\top$ and oriented at ϕ can be decomposed into translation to the origin, followed by isotropic scaling s, rotation by ϕ, and translation to $[x_B, y_B]^\top$. The transformation of points $[x, y]^\top$ can be thus expressed in homogeneous coordinates by $\mathbf{T_{UB}} \cdot [x, y, 1]^\top$ where

$$\mathbf{T_{UB}} = \begin{bmatrix} 1 & 0 & x_B \\ 0 & 1 & y_B \\ 0 & 0 & 1 \end{bmatrix} \cdot \begin{bmatrix} s & 0 & 0 \\ 0 & s & 0 \\ 0 & 0 & 1 \end{bmatrix} \cdot \begin{bmatrix} \cos(\phi) & -\sin(\phi) & 0 \\ \sin(\phi) & \cos(\phi) & 0 \\ 0 & 0 & 1 \end{bmatrix} \cdot \begin{bmatrix} 1 & 0 & -x_U \\ 0 & 1 & 0 \\ 0 & 0 & 1 \end{bmatrix}. \tag{25}$$

To mitigate errors potentially arising from the numerical fitting of the two ellipses we obtain the isotropic scale as the averaged axes ratio $s = \frac{1}{2}(||\vec{a_B}||/||\vec{a_U}|| + ||\vec{b_B}||/||\vec{b_U}||)$.